

## REVISITING THE LONG/SOFT – SHORT/HARD CLASSIFICATION OF GAMMA-RAY BURSTS IN THE FERMI ERA

FU-WEN ZHANG<sup>1,2,3</sup>, LANG SHAO<sup>4</sup>, JING-ZHI YAN<sup>1,2</sup>, AND DA-MING WEI<sup>1,2</sup>

*Draft version August 13, 2018*

### ABSTRACT

We perform a statistical analysis of the temporal and spectral properties of the latest Fermi gamma-ray bursts (GRBs) to revisit the classification of GRBs. We find that the bimodalities of duration and the energy ratio ( $E_{\text{peak}}/\text{Fluence}$ ) and the anti-correlation between spectral hardness (hardness ratio ( $HR$ ), peak energy and spectral index) and duration ( $T_{90}$ ) support the long/soft – short/hard classification scheme for Fermi GRBs. The  $HR - T_{90}$  anti-correlation strongly depends upon the spectral shape of GRBs and energy bands, and the bursts with the curved spectra in the typical BATSE energy bands show a tighter anti-correlation than those with the power-law spectra in the typical BAT energy bands. This might explain why the  $HR - T_{90}$  correlation is not evident for those GRB samples detected by instruments like *Swift* with a narrower/softer energy bandpass. We also analyze the intrinsic energy correlation for the GRBs with measured redshifts and well defined peak energies. The current sample suggests  $E_{\text{p,rest}} = 2455 \times (E_{\text{iso}}/10^{52})^{0.59}$  for short GRBs, significantly different from that for long GRBs. However, both the long and short GRBs comply with the same  $E_{\text{p,rest}} - L_{\text{iso}}$  correlation.

*Subject headings:* gamma-rays burst: general - methods: data analysis

### 1. INTRODUCTION

The field of gamma-ray bursts (GRBs) has rapidly advanced in recent years especially after the launch of NASA missions *Swift* (in 2004, Gehrels et al. 2004) and *Fermi* (in 2008, Atwood et al. 2009). A physical classification of GRBs is still a basic open question (e.g., Zhang 2011). According to the traditional classification schemes, GRBs can be divided into long and short ones, based on the well-known bimodal distribution of their durations monitored by the Burst And Transient Source Experiment (BATSE, Meegan et al. 1992), which also show different spectral hardness ratios ( $HR$ ; Kouveliotou et al. 1993). The  $HR$  in conjunction with the duration provides a means for classification, e.g., the long/soft class comprises roughly 3/4 of the population and the short/hard class comprises the other 1/4 for BATSE GRBs (Kouveliotou et al. 1993; Qin et al. 2000). The difference between long and short GRBs is further established by the observations of afterglows and host galaxies. The fact that several nearby long GRBs are associated with Type Ic Supernovae (SNe) and most long GRB host galaxies are found be dwarf star-forming galaxies favors the speculation that most long GRBs are accompanied by massive stellar explosions (see Woosley & Bloom 2006, for a review). Some nearby short GRBs (or short GRBs with a long-soft extended emission) have host galaxies that are elliptical or of early type, with little star formation (Fox et al. 2005; Gehrels et al. 2005; Berger et al. 2005a; Barthelmy et al. 2005). This points towards a different type of progenitor, e.g. compact object mergers (see Nakar 2007, for a review).

This dichotomous picture was soon challenged by some following observations. GRB 060614 and GRB 060505 are

two nearby long GRBs that did not have bright SN associations, sharing similar properties to short GRBs (Fynbo et al. 2006; Della Valle et al. 2006; Xu et al. 2009). Three high- $z$  GRBs 080913, 090423 and 090429B have rest-frame durations shorter than 1 s, but are likely related to massive stars<sup>5</sup> (Greiner et al. 2009; Salvaterra et al. 2009; Tanvir et al. 2009; Cucchiara et al. 2011). An observed short GRB 090426 was found in many aspects similar to long GRBs and it was also probably linked to the death of a massive star (Antonelli et al. 2009; Levesque et al. 2010; Xin et al. 2011; Thöne et al. 2011; Nicuesa Guelbenzu et al. 2011). These results suggest that certain observational properties (e.g., long vs. short duration) do not always refer to certain types of progenitor (see Zhang et al. 2009 and the references therein). Moreover, the bimodal duration distribution was not presented in observation for some detectors with a narrow/softer energy bandpass such as HETE-2 and *Swift*, and the distinction of short/hard and long/soft in the hardness-duration panel is not very clear (e.g., Sakamoto et al. 2011 and the references therein; Shao et al. 2011). Recently, Guiriec et al. (2010) analyzed 3 very bright short GRBs observed by the Fermi Gamma-Ray Burst Monitor (GBM, Meegan et al. 2009), and found that short GRBs are very similar to long ones, but with light curves contracted in time and with harder spectra stretched toward higher energies. They also showed that the hardness evolutions during the bursts follow their flux/intensity variations, similar to long bursts. By studying the composite light curves including both the prompt and afterglow emission of GRBs detected by *Swift*, Shao et al. (2011) found the similarity of the radiative features between the long and short bursts. They also proposed that the spectral evolution of the prompt emission might be an important factor that determines the correlation between the hardness ratio and duration.

Theoretically speaking, the duration may be not an unique indicator for the physical category of a GRB. In the pre-*Swift* era, it was already known that (1) the coalescence of two compact objects can produce either long or short GRBs, depend-

fwzhang@pmo.ac.cn(F.-W.Z.)

<sup>1</sup> Purple Mountain Observatory, Chinese Academy of Sciences, Nanjing 210008, China;

<sup>2</sup> Key Laboratory of Dark Matter and Space Astronomy, Chinese Academy of Sciences, Nanjing 210008, China;

<sup>3</sup> College of Science, Guilin University of Technology, Guilin 541004, China;

<sup>4</sup> Department of Physics, Hebei Normal University, Shijiazhuang 050016, China.

<sup>5</sup> The other possibility that these high redshift bursts may be from the super-conducting cosmic strings has been tightly constrained (Wang et al. 2011).

ing on the remnant formed in the merger (a short burst is likely if the remnant is a stellar black hole while a long burst is expected if the remnant is a super-massive neutron star; see Kluzniak & Ruderman 1998 and the references therein); (2) the collapse of a massive star usually produces long GRBs but the possibility of generating short events can not be ruled out (Zhang et al. 2003; Fan et al. 2005). One may appeal to multiple observational criteria to judge the correct physical category of the GRB progenitor model that is associated with a certain GRB (e.g., Zhang et al. 2009; Fan et al. 2005; Kann et al. 2011). Recently, Goldstein et al. (2010) found that the distribution of the  $E_{\text{peak}}/\text{Fluence}$  energy ratio has a clear bimodality by analyzing the complete BATSE 5B Spectral Catalog. An obvious distinction between long and short bursts emerges from this bimodal distribution. This result was further confirmed by an analysis of 382 GRBs from the GBM spectral catalog (Goldstein et al. 2011). Another phenomenological classification method for GRBs was proposed by Lü et al. (2010).

It is urgent to discuss the classification issues further in the Fermi era. The preliminary analysis results of GRBs observed by Fermi-GBM presented by e.g., Bissaldi et al. (2011), Nava et al. (2011, hereafter N11), and Shao et al. (2011) confirmed the duration bimodality found in the BATSE data (Kouveliotou et al. 1993). Whether the hardness-duration correlation is also consistent with the BATSE result and the short/hard – long/soft dichotomy classification scheme is robust have not been explored yet. In this paper, we present a systematic analysis of the temporal and spectral properties of Fermi-GBM GRBs catalogued by N11 and analyze the intrinsic energy correlation of GRBs with measured redshift and well defined peak energy. This paper is structured as follows. The data and sample are presented in Section 2. In Section 3, we revisit the distribution of duration, the correlation between hardness and duration, the distribution of energy ratio and the intrinsic energy correlation. In Section 4, we give a summary.

## 2. DATA AND SAMPLE

The Fermi-GBM detected 438 GRBs by the end of March 2010. The spectral properties of these GRBs have been analyzed and published by N11. Out of the 432 GRBs for which it was possible to perform the spectral analysis, 323 bursts have curved spectra which are well fitted by the Band (Band et al. 1993) or by a cut-off power law (CPL) model. The remaining 109 bursts are best fitted with a simple power-law. In addition, the peak flux spectra of 235 bursts could be extracted and fitted with a Band or CPL model. The detailed data extraction and analysis can be found in the catalog by N11, which we adopted in the following analysis. Recently, the first two years Fermi-GBM GRB catalog was released (see, Paciesas et al. 2012; Goldstein et al. 2012). The duration ( $T_{90}$ ) of 487 GRBs are reported in the catalog. Combined with the duration data, we separate the 427 GRBs with an analyzed spectrum into different samples (5 cases are not included for lack of  $T_{90}$  data): 322 GRBs with the curved spectra (Band or CPL model) represent *sample 1*, while 103 GRBs with the power-law spectra represent *sample 2*<sup>6</sup>. Furthermore, the 234 GRBs with a fitted peak flux spectrum represent *sample 3* (one burst without  $T_{90}$  data is excluded).

To analyze the intrinsic energy correlation of the different GRB classes, we collect the GRBs with known redshift and

well defined peak energy up to the end of May 2011. This sample includes 110 long GRBs and 7 short GRBs detected by BeppoSAX, HETE-2, Swift, Suzaku and Fermi. Most of data are taken from Amati et al. (2008, 2009), Nava et al. (2008), Ghirlanda et al. (2009, 2010) and the references therein, as well as the GRB Coordinates Network (GCN). The isotropic gamma-ray energy ( $E_{\text{iso}}$ ) and luminosity ( $L_{\text{iso}}$ ) are calculated in the rest frame in the energy range 1 – 10000 keV.

## 3. TEMPORAL AND SPECTRAL ANALYSIS

### 3.1. Duration and Hardness

Distribution of duration is crucial for the traditional GRB classification. We analyze the distribution of durations of Fermi GRBs in N11 catalog in detail. As shown in Figure 1, the duration distributions are bimodal either for all the bursts or for samples 1 and 2. The “short” and “long” GRBs are well separated in the log-normal plot, which is consistent with the previous findings (e.g., Bissaldi et al. 2011; N11; Shao et al. 2011). For all the GRBs in N11, we find a central value  $\mu_1 = -0.23$  (i.e.,  $T_{90} \sim 0.59$  s; with a standard deviation  $\sigma_1 = 0.47$ ) and  $\mu_2 = 1.42$  (i.e.,  $T_{90} \sim 26.3$  s; with a standard deviation  $\sigma_2 = 0.47$ ) for short and long bursts, respectively. For *sample 1* and *sample 2*, the best fits yield  $\mu_1 = -0.36$  ( $T_{90} \sim 0.44$  s;  $\sigma_1 = 0.46$ ) and  $\mu_2 = 1.47$  ( $T_{90} \sim 29.5$  s;  $\sigma_2 = 0.47$ ) and  $\mu_1 = -0.23$  ( $T_{90} \sim 0.59$  s;  $\sigma_1 = 0.22$ ) and  $\mu_2 = 1.04$  ( $T_{90} \sim 11$  s;  $\sigma_2 = 0.57$ ), respectively. These results show that the duration bimodality is not affected by the spectral shape of GRBs, but the duration central value of long bursts in *sample 2* is shifted to smaller value and the duration distribution covers a smaller range (see the middle panel of Figure 1). In other words, on average, the duration of long GRB with power-law spectrum is smaller than that of GRB with curved spectrum. It is well known that the duration strongly depends upon the sensitivity and the energy range of the instrument. The bimodal distribution of duration is either a robust result or a instrument selection effect. Using the data of GRBs simultaneously detected by Swift-BAT and Fermi-GBM, Virgili et al. (2011) found that the duration distributions in the BAT and GBM bands are all bimodal. It is essential to make a more detailed study explaining the fact that the bimodal duration distribution is not presented in observations of HETE-2 and Swift. The future work is going to explore it. We also adopt the conventional  $T_{90} = 2$  s to separate short and long GRBs.

The spectral hardness is an additional discriminator for the classification of GRBs. In this work, we firstly explore the correlation between  $HR$  and  $T_{90}$ , where  $HR$  defines the fluence ratio between two broad energy bands. We simply divide the GBM energy band (10-1000 keV) into five energy bands, i.e. 10-25, 25-50, 50-100, 100-300, 300-1000 keV. Using the spectral data in N11, we are able to calculate  $HR$  in arbitrary two energy bands. We define four different  $HR$  measurements, namely  $HR1$ , between the 50-100 keV and the 25-50 keV energy bands, i.e. the typical BAT energy bands;  $HR2$ , between the 100-300 keV and the 50-100 keV energy bands, i.e. the typical BATSE energy bands;  $HR3$ , between the 300-1000 keV and the 10-300 keV energy bands; and  $HR4$ , between the 100-1000 keV and the 25-100 keV energy bands.

We find that the values of  $HR$  are significantly different in these energy bands. This is expected, since they strongly depend on the energy bands between which they are calculated. Figure 2 shows  $HR$  versus  $T_{90}$  for 425 GRBs from N11. From this figure, we find that there is an obvious tendency that short

<sup>6</sup> The two GRBs with unusually soft spectra ( $\alpha = -3.52$  for GRB 100112 and  $\alpha = -3.98$  for GRB 100207) are excluded in the analysis.

GRBs have harder spectra than long GRBs. The correlations between  $HR$  and  $T_{90}$  are reported in Table 1. We find that (1) for all 425 GRBs,  $HR$  and  $T_{90}$  are all anti-correlated for all choices of  $HR$  ( $HR1$ - $HR4$ ), but the correlation coefficients as well as the slopes are different; (2) the values of  $HR$  are larger and the  $HR - T_{90}$  anti-correlation is stronger in the typical BATSE energy bands (the median value of  $HR$  is 2.21, the correlation coefficient is  $r = -0.41$ , the chance probability is  $p = 2.8 \times 10^{-18}$ , and the slope is  $b = -0.12$ ) than those in the BAT energy bands (the median value of  $HR$  is 1.56,  $r = -0.28$ ,  $p = 5.2 \times 10^{-9}$ , and  $b = -0.06$ ); (3) if we consider short and long GRBs separately, the correlations are very weak or even negligible.

In addition, the question arises whether the  $HR - T_{90}$  anti-correlation of GRBs depends on spectral shapes. For a comparison with the previous results from the BASTE and BAT observations, the correlations between  $HR1$  and  $T_{90}$ , and between  $HR2$  and  $T_{90}$  for *sample 1* and *sample 2* are investigated. The results are shown in Figure 3 and Table 1. We find that the anti-correlation between  $HR$  and  $T_{90}$  indeed depends on the spectral shape of GRBs, and the GRBs with the curved spectra have a more clear correlation than those with the power-law spectra in the same energy bands (for a detailed analysis, see Table 1). Now, the fact that there is no obvious correlation between  $HR$  and  $T_{90}$  in the Swift-BAT sample as well as other samples detected by instruments with a narrow/softer energy bandpass such as HETE-2 (Sakamoto et al. 2011) can be easily understood. This is because (1) the  $HR - T_{90}$  anti-correlation depends upon the energy bands and the correlation in the typical BAT energy bands is weak; (2) the majority of spectra of BAT GRBs are best fitted by a single power-law model. This is due to the fact that BAT only covers a narrow energy band. The  $HR - T_{90}$  anti-correlation for GRBs with the power-law spectra is not obvious; (3) for a given GRB sample, the values of  $HR$  are small and the values of  $T_{90}$  are large for BAT-like softer detector, this makes the  $HR - T_{90}$  anti-correlation unclear.

The peak energy and spectral index are also usually adopted to depict the hardness of GRBs. N11 found that, on average, short GRBs have a higher peak energy ( $\sim 490$  keV) and a harder low-energy spectral index ( $\sim -0.50$ ) than long GRBs ( $\sim 160$  keV and  $\sim -0.92$ ). We analyze the correlations between  $E_{\text{peak}}$  (peak energy in the time integrated spectra) and  $T_{90}$ , and between  $E_{\text{peak}}^p$  (peak energy in the peak flux spectra) and  $T_{90}$  for *sample 1*, and between  $\alpha$  (which represents the spectral index of GRBs best fitted with a power-law model) and  $T_{90}$  for *sample 2*. The results are shown in Figures 4 and 5. We find that  $E_{\text{peak}}$  and  $T_{90}$ ,  $E_{\text{peak}}^p$  and  $T_{90}$ ,  $\alpha$  and  $T_{90}$  are all anti-correlated. The detailed correlation analysis are presented in Table 2. The fact that short GRBs have harder spectra and long GRBs have softer spectra is confirmed once again. Recently, Gruber et al. (2011) suggested that the rest frame peak energy distributions might be the same for the two classes of GRBs based on a small Fermi GRB sample with measured redshift. The different redshift distribution of the two classes of GRBs might be responsible for the different distributions of the observed peak energies (see e.g. Guetta & Piran 2005). However, we also should note that the redshift distribution which has been found to be different for long and short GRBs might have been strongly affected by the measurement methods. Short GRBs tend to have lower redshift, very similar to those of long GRBs measured by the same method, i.e., spectral analysis of the presumed host galaxies

(Shao et al. 2011). Therefore, the distribution of the intrinsic peak energy of the two classes of GRBs and the  $E_{\text{peak}} - T_{90}$  anti-correlation are needed to a further confirm. Moreover, for the short and long classes separately, the  $E_{\text{peak}} - T_{90}$ ,  $E_{\text{peak}}^p - T_{90}$ , and  $\alpha - T_{90}$  anti-correlations do not exist or even are positive correlated. These results are consistent with what was found from the analysis of the correlation between  $HR$  and  $T_{90}$ . Our results indicate that hardness ratio, peak energy and spectral index might be linked to the same physical feature of GRBs. The nature is unknown so far.

### 3.2. Distribution of Energy Ratio

Although the distributions of hardness and duration can be used to classify GRBs, the overlap between these two classes of GRBs can not be ignored. Moreover, this scheme strongly relies on the subjective choices required for the duration calculation. Recently, Goldstein et al. (2010) showed that the  $E_{\text{peak}}/\text{Fluence}$  energy ratio (which physically represents a ratio of the energy at which most of the gamma rays are emitted to the total energy emitted in gamma rays) can be used as a new GRB classification discriminator. This also has the big advantage that it does not rely on the burst duration estimate. Using the preliminary duration and spectral result of 382 Fermi-GBM GRBs, Goldstein et al. (2011) analyzed the distribution of energy ratio and found that the distribution separated into long bursts and short bursts well. This supports the original claim obtained by Goldstein et al. (2010). Meanwhile, we also analyze the distribution of the energy ratio for *sample 1*. The fluence in the 10–1000 keV energy band is calculated by using the spectral parameters in N11, then we obtain the values of  $E_{\text{peak}}/\text{Fluence}$  for each of GRBs in *sample 1*. Figure 6 shows the distribution of the energy ratio. In the top panel, we plot the 316 GRBs included in our *sample 1*. A bimodal distribution is evident, as previously shown by Goldstein et al. (2011). By using a standard nonlinear least-squares fitting algorithm, we fit the distribution by two log-normal functions. The best fits yield a central value  $\mu_1 = -1.34$  with a standard deviation  $\sigma_1 = 0.62$ , and  $\mu_2 = 0.27$  with  $\sigma_2 = 0.35$ , respectively. In the bottom panel of Figure 6, we present two distributions corresponding to long (unfilled histogram) and short (filled histogram) GRBs. This further confirms the fact that (1) the bimodality of the energy ratio distribution is correlated to that of the burst duration, and that (2) the energy ratio is indeed a good discriminator for classifying GRBs. Indeed, it could be used to identify some of the controversial GRBs previously discussed (see Section 3.3). The energy ratio bimodality can also be easily understood if we note that short GRBs tend to have larger peak energies and smaller fluences (due to their short durations) with respect to the long ones.

To further check the differences between long and short GRBs, we investigate the correlations between the peak flux ( $P$ ) and  $T_{90}$  and between the  $E_{\text{peak}}^p/P$  ratio (which physically represents a ratio of the energy at which most of the gamma rays are emitted to the total energy emitted in gamma rays in one second at peak of a burst) and  $T_{90}$ . Those two quantities namely do not depend on the duration of a burst. The detailed results are presented in Figure 7 and Table 2. Both the correlations between  $P$  and  $T_{90}$  and between  $E_{\text{peak}}^p/P$  and  $T_{90}$  (shown in the top and bottom panel of Figure 7, respectively) are different for long and short GRBs. An anti-correlation between  $P$  and  $T_{90}$  and a positive correlation between  $E_{\text{peak}}^p/P$  and  $T_{90}$  are found for all 234 GRBs with the peak flux curved spectra, although the correlations are not very strong. Likewise, if

we consider short and long classes separately, the correlations are negligible or even reversed. This further confirm that the correlation between the hardness and the duration of GRBs is only a general trend between two clusters of GRBs or two types of GRBs and does not apply to either type.

### 3.3. Intrinsic Spectral Energy Correlation

Amati et al. (2002) found a tight correlation between the rest frame peak energy,  $E_{p,\text{rest}}$  and the isotropic equivalent gamma-ray energy,  $E_{\text{iso}}$ , which was confirmed by later observations (Amati 2006, 2010). However, short GRBs do not follow the correlation, as is true for the peculiarly sub-energetic and close GRB 980425, the proto-type of the GRB/SN connection (e.g., Amati 2006, 2010; Piranomonte et al. 2008; Ghirlanda et al. 2009, Gruber et al. 2011). These facts suggest that the  $E_{p,\text{rest}} - E_{\text{iso}}$  plane may be used to distinguish between different classes of GRBs and to understand the differences in the physics/geometry of their emission. Here we reanalyze this correlation taking into account the new observational data. Only 7 short GRBs with redshift, reliable estimate of  $E_{\text{peak}}$  and other spectral parameters are available by the end of May 2011, as listed in Table 2.

The three peculiar/controversial short GRBs (GRBs 071227, 090927 and 100816A; Piranomonte et al. 2008; Amati et al. 2010; Gruber et al. 2011) are excluded for the following reasons. Caito et al. (2010) suggested that GRB 071227 represents another example of a disguised short GRB, after GRB 970228 and GRB 060614, on the basis of their analysis performed in the context of the fireshell scenario. GRB 090927 and GRB 100816A are two short GRBs detected by Fermi and had been analyzed by Gruber et al. (2011). However the spectrum of GRB 090927 is adequately fitted by a simple power law function (see, Gruber et al. 2009; Nava et al. 2011), which has been confirmed by our current analysis. The category of this GRB hence can not be further identified due to its inaccurate peak energy measurement. GRB 100816A was simultaneously detected by Swift-BAT, Fermi-GBM and Konus-Wind, and its duration estimated by these three missions is  $2.9 \pm 0.6$  s (15-350 keV), 2 s (50-300 keV) and  $\sim 2.8$  s (20 keV-2 MeV), respectively. So it is difficult to determine whether this GRB belongs to the short or to the long class only based on its duration. Fan & Wei (2011) identified a possible wind-like medium surrounding this burst, which suggested a massive star origin (i.e., this short-like GRB should be a long one). Moreover, this GRB does not deviate from the  $E_{p,\text{rest}} - E_{\text{iso}}$  region of long GRBs (see also Gruber et al. 2011). We calculate the energy ratio and obtain  $\log(E_{\text{peak}}/\text{Fluence}) = -1.24$  for GRB 100816A, which is a typical value of long GRBs. Therefore, this event should belong to the long class and has been included in our long GRB sample.

We also collected GRBs observed by Fermi-GBM with the same standard as short GRBs analyzed above from the GCN. 27 GRBs (including two short ones listed in Table 2) are obtained, as listed in Table 3. Using the same calculation method as Amati et al. (2008), we obtain their isotropic equivalent energies in the energy range 1-10000 keV (in the bursts' rest frame). Figure 8 shows the correlation between  $E_{p,\text{rest}}$  and  $E_{\text{iso}}$ . Data reported in Amati et al. (2010) and the references therein are also included. We find that the short GRBs are significantly different from the long ones. To obtain a quantitative comparison, we fit the  $E_{p,\text{rest}} - E_{\text{iso}}$  correlations for the

short and long GRBs separately. The best fits yield

$$E_{p,\text{rest}} = 2455 \times \left(\frac{E_{\text{iso}}}{10^{52}}\right)^{0.59 \pm 0.04} \text{ for short GRBs,}$$

with a spearman's rank correlation coefficient  $r = 0.89$  and a chance probability  $P = 6.8 \times 10^{-3}$ , and

$$E_{p,\text{rest}} = 100 \times \left(\frac{E_{\text{iso}}}{10^{52}}\right)^{0.51 \pm 0.03} \text{ for long GRBs,}$$

with  $r = 0.85$  and  $P = 1.2 \times 10^{-31}$  (see Table 1). For long GRBs, the result is in agreement with that obtained by some authors (e.g., Amati 2010; Ghirlanda et al. 2009; 2010; Gruber et al. 2011).

Wei & Gao (2003) discovered a tight correlation between the rest frame peak energy and the luminosity ( $L_{\text{iso}}$ ) based on nine GRBs (see their Fig.6). Such a correlation was soon confirmed by others (e.g., Yonetoku et al. 2004; Ghirlanda et al. 2005). Recently, further studies showed that although short GRBs are inconsistent with the  $E_{p,\text{rest}} - E_{\text{iso}}$  correlation hold by long GRBs, they might follow the  $E_{p,\text{rest}} - L_{\text{iso}}$  correlation (e.g., Ghirlanda et al. 2009; Gruber et al. 2011). Such a trend has been confirmed by our analysis with the latest data<sup>7</sup> (see Figure 9). The fit to the  $E_{p,\text{rest}} - L_{\text{iso}}$  correlation yields

$$E_{p,\text{rest}} = 302 \times \left(\frac{L_{\text{iso}}}{10^{52}}\right)^{0.40 \pm 0.03},$$

with  $r = 0.76$  and  $P = 2.3 \times 10^{-23}$ . This might imply that the energy dissipation processes powering the prompt gamma-ray emission of short and long GRBs are rather similar though the progenitors of these two kinds of events are likely different.

## 4. SUMMARY

In this work, we perform a statistical analysis of the temporal and spectral properties of the latest Fermi-GBM GRBs catalogued by N11 to revisit the classification of GRBs. The traditional short/hard and long/soft classification is supported for these Fermi GRBs by the following facts: (1) The duration of the prompt gamma-ray emission has a clear bimodal distribution. (2) The energy ratio (i.e.,  $E_{\text{peak}}/\text{Fluence}$ ) also has a clear bimodal distribution and its bimodality is correlated to that of the duration distribution. (3) The anti-correlation between spectral hardness (hardness ratio, peak energy, and spectral index) and duration is also confirmed. Moreover, we find out that the correlation between the hardness and the duration is only a general trend between two clusters of GRBs or two types of GRBs and does not apply to either type. Interestingly there are two leading models for GRBs. One is the collapsar that likely produces long-lasting GRBs. The other is the merger of two compact objects which is expected to power short-living GRBs. However, it is not always reasonable to argue a collapsar origin for long bursts and a merger origin for short bursts since the possibilities that the collapsar can also produce short GRBs and the merger can generate long GRBs can not be ruled out, as already realized in the pre-Swift era (e.g., Kluźniak & Ruderman 1998; Zhang et al. 2003; Fan et al. 2005). The observations of some Swift GRBs, such as GRB 060614 and GRB 080503 (e.g., Xu et al. 2009), partly confirm such speculations. Therefore additional discriminators are highly needed to classify GRBs reliably.

<sup>7</sup> The long GRB data are taken from Ghirlanda et al. 2010 and the references therein.

In this work we also find that the anti-correlation between hardness ratio and duration depends upon the spectral shapes of GRBs and the energy bands. The bursts with the curved spectra in the typical BATSE energy bands (between the 100-300 keV and the 50-100 keV bands) show a tighter anti-correlation than those with the power-law spectra in the typical BAT energy bands (between the 50-100 keV and the 25-50 keV bands). This might explain why the  $HR - T_{90}$  correlation is not evident for Swift-BAT GRB sample as well as other GRB sample detected by instruments with a narrow/softer energy bandpass such as HETE-2 (e.g., Sakamoto et al. 2011, Shao et al. 2011). We also analyze the intrinsic energy correlation for the different GRB classes and find that all short GRBs deviate significantly from the  $E_{p,rest} - E_{iso}$  correlation

hold by long GRBs, and they might follow another one

$$E_{p,rest} = 2455 \times (E_{iso}/10^{52})^{0.59}$$

based on the current small sample. The future observation will test our result.

We are grateful to L. Nava for providing the published Fermi-GBM data in their work. We acknowledge the GBM team for the public distribution of the spectral properties of Fermi-GBM GRBs through the GCN network. We also thank Dr. Yi-Zhong Fan for stimulating discussion. This work was supported in part by the National Natural Science Foundation of China (grants 10973041, 10921063, 11163003 and 11103083) and the National Basic Research Program of China (No. 2007CB815404). F.-W.Z. acknowledges the support by the China Postdoctoral Science Foundation funded project (No. 20110490139), the Guangxi Natural Science Foundation (No. 2010GXNSFB013050) and the doctoral research foundation of Guilin University of Technology.

## REFERENCES

- Amati, L. 2006, MNRAS, 372, 233  
 Amati, L. 2010, arXiv:1002.2232  
 Amati, L., et al. 2002, A&A, 390, 81  
 Amati, L., Frontera, F., & Guidorzi, C. 2009, A&A, 508, 173  
 Amati, L., Guidorzi, C., Frontera, F., Della Valle, M., Finelli, F., Landi, R., & Montanari, E. 2008, MNRAS, 391, 577  
 Antonelli, L. A., et al. 2009, A&A, 507, L45  
 Atwood, W. B., Abdo, A. A., Ackermann, M., et al. 2009, ApJ, 697, 1071  
 Band, D., et al. 1993, ApJ, 413, 281  
 Barthelmy, S. D., et al. 2005, Nature, 438, 994  
 Berger, E., et al. 2005a, Nature, 438, 988  
 Bissaldi, E., et al. 2011, ApJ, 733, 97  
 Caito, L., Amati, L., Bernardini, M. G., Bianco, C. L., de Barros, G., Izzo, L., Patricelli, B., & Ruffini, R. 2010, A&A, 521, A80  
 Cucchiara, A., et al. 2011, ApJ, 736, 7  
 Della Valle, M., et al. 2006, Nature, 444, 1050  
 Fan, Y.-Z., & Wei, D.-M. 2011, ApJ, 739, 47 (arXiv:1107.2656)  
 Fan, Y. Z., Zhang, B., Kobayashi, S., & Mészáros, P. 2005, ApJ, 628, 867  
 Fox, D. B., et al. 2005, Nature, 437, 845  
 Frontera, F., et al. 2009, ApJS, 180, 192  
 Fynbo, J. P. U., et al. 2006, Nature, 444, 1047  
 Gehrels, N., et al. 2004, ApJ, 611, 1005  
 Gehrels, N., et al. 2005, Nature, 437, 851  
 Ghirlanda, G. 2011, IAU Symposium, 275, 344  
 Ghirlanda, G., Ghisellini, G., Nava, L., & Burlon, D. 2011b, MNRAS, 410, L47  
 Ghirlanda, G., Ghisellini, G., & Nava, L. 2011a, MNRAS, L336  
 Ghirlanda, G., Nava, L., & Ghisellini, G. 2010, A&A, 511, A43  
 Ghirlanda, G., Nava, L., Ghisellini, G., Celotti, A., & Firmani, C. 2009, A&A, 496, 585  
 Ghirlanda, G., Nava, L., Ghisellini, G., Firmani, C., & Cabrera, J. I. 2008, MNRAS, 387, 319  
 Golenetskii, S., Aptekar, R., Mazets, E., et al. 2007, GRB Coordinates Network, 7155, 1  
 Golenetskii, S., Aptekar, R., Frederiks, D., et al. 2010, GRB Coordinates Network, 11470, 1  
 Goldstein, A., Preece, R. D., & Briggs, M. S. 2010, ApJ, 721, 1329  
 Goldstein, A., Preece, R. D., Briggs, M. S., et al. 2011, arXiv:1101.2458  
 Goldstein, A., Burgess, J. M., Preece, R. D., et al. 2012, arXiv:1201.2981  
 Greiner, J., et al. 2009, ApJ, 693, 1610  
 Gruber, D., Bissaldi, E., & McBreen, S. 2009, GRB Coordinates Network, 9974, 1  
 Gruber, D., et al. 2011, A&A, 531, A20  
 Guetta, D., & Piran, T. 2005, A&A, 435, 421  
 Guiriec, S., Connaughton, V., & Briggs, M. 2009, GRB Coordinates Network, 9336, 1  
 Guiriec, S., Briggs, M. S., Connaughton, V., et al. 2010, ApJ, 725, 225  
 Kann, D. A., Klose, S., Zhang, B., et al. 2011, ApJ, 734, 96  
 Kann, D. A., Klose, S., Zhang, B., et al. 2010, ApJ, 720, 1513  
 Kluźniak, W., & Ruderman, M. 1998, ApJ, 505, L113  
 Kouveliotou, C., et al. 1993, ApJ, 413, L101  
 Levesque, E. M., et al. 2010, MNRAS, 401, 963  
 Lü, H.-J., Liang, E.-W., Zhang, B.-B., & Zhang, B. 2010, ApJ, 725, 1965  
 Meegan, C. A., Fishman, G. J., Wilson, R. B., et al. 1992, Nature, 355, 143  
 Meegan, C., Lichti, G., Bhat, P. N., et al. 2009, ApJ, 702, 791  
 Nakar, E. 2007, Phys. Rep., 442, 166  
 Nava, L., Ghirlanda, G., Ghisellini, G., & Firmani, C. 2008, MNRAS, 391, 639  
 Nava, L., Ghirlanda, G., Ghisellini, G., & Celotti, A. 2011a, A&A, 530, A21 (N11)  
 Nava, L., Ghirlanda, G., Ghisellini, G., & Celotti, A. 2011b, MNRAS, 415, 3153  
 Nicuesa Guelbenzu, A., et al. 2011, A&A, 531, L6  
 Paciesas, W. 2010, GRB Coordinates Network, 10345, 1  
 Paciesas, W. S., Meegan, C. A., von Kienlin, A., et al. 2012, arXiv:1201.3099  
 Piranomonte, S., et al. 2008, A&A, 491, 183  
 Qin, Y.-P., Xie, G.-Z., Xue, S.-J., Liang, E.-W., Zheng, X.-T., & Mei, D.-C. 2000, PASJ, 52, 759  
 Sakamoto, T., et al. 2011, ApJS, 195, 2  
 Salvaterra, R., et al. 2009, Nature, 461, 1258  
 Shao, L., Dai, Z.-G., Fan, Y.-Z., Zhang, F.-W., Jin, Z.-P., & Wei, D.-M. 2011, ApJ, 738, 19  
 Tanvir, N. R., et al. 2009, Nature, 461, 1254  
 Thöne, C. C., et al. 2011, MNRAS, 414, 479  
 Virgili, F., Qin, Y., Zhang, B., & Liang, E. 2011, arXiv:1112.4363  
 Wang, Y., Fan, Y. Z. & Wei, D. M. 2011, Phys. Rev. Lett., 106, 259001  
 Wei, D. M., & Gao, W. H. 2003, MNRAS, 345, 743  
 Woosley, S. E., & Bloom, J. S. 2006, ARA&A, 44, 507  
 Xin, L.-P., et al. 2011, MNRAS, 410, 27  
 Xu, D., Starling, R. L. C., Fynbo, J. P. U., et al. 2009, ApJ, 696, 971  
 Yonetoku, D., Murakami, T., Nakamura, T., Yamazaki, R., Inoue, A. K., & Ioka, K. 2004, ApJ, 609, 935  
 Zhang, B., et al. 2009, ApJ, 703, 1696  
 Zhang, B. 2011, Comptes Rendus Physique, 12, 206  
 Zhang, W., Woosley, S. E., & MacFadyen, A. I. 2003, ApJ, 586, 356

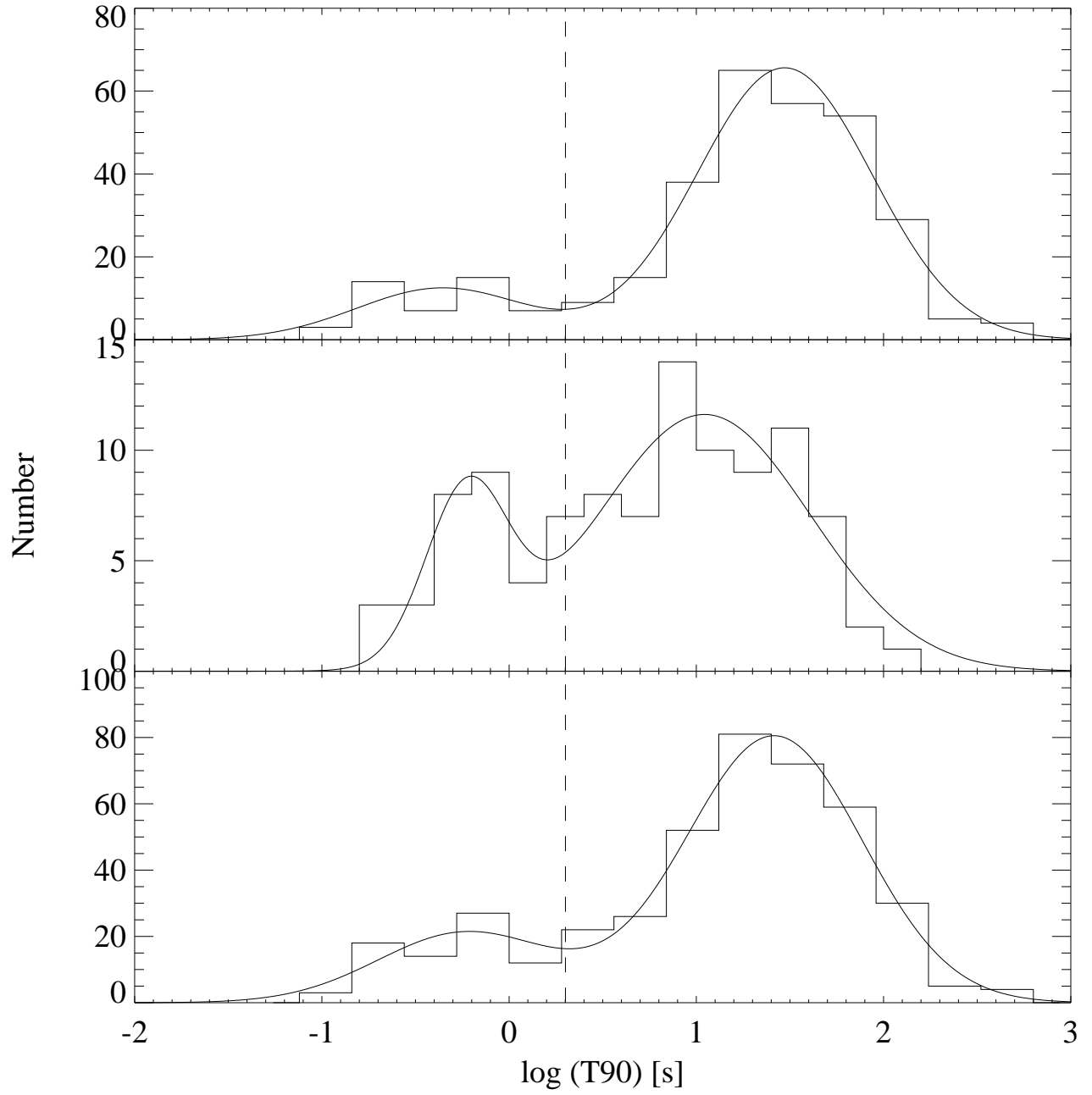


FIG. 1.— Distributions of the durations for 322 GRBs with the curved spectra (*sample 1*, top panel), 103 GRBs with the power-law spectra (*sample 2*, middle panel), and all 425 GRBs (bottom panel) observed by Fermi. The solid lines show the best fits with two log-normal functions and the dashed vertical line is 2 s separation line. The  $T_{90}$  data are taken from Paciesas et al. 2012.

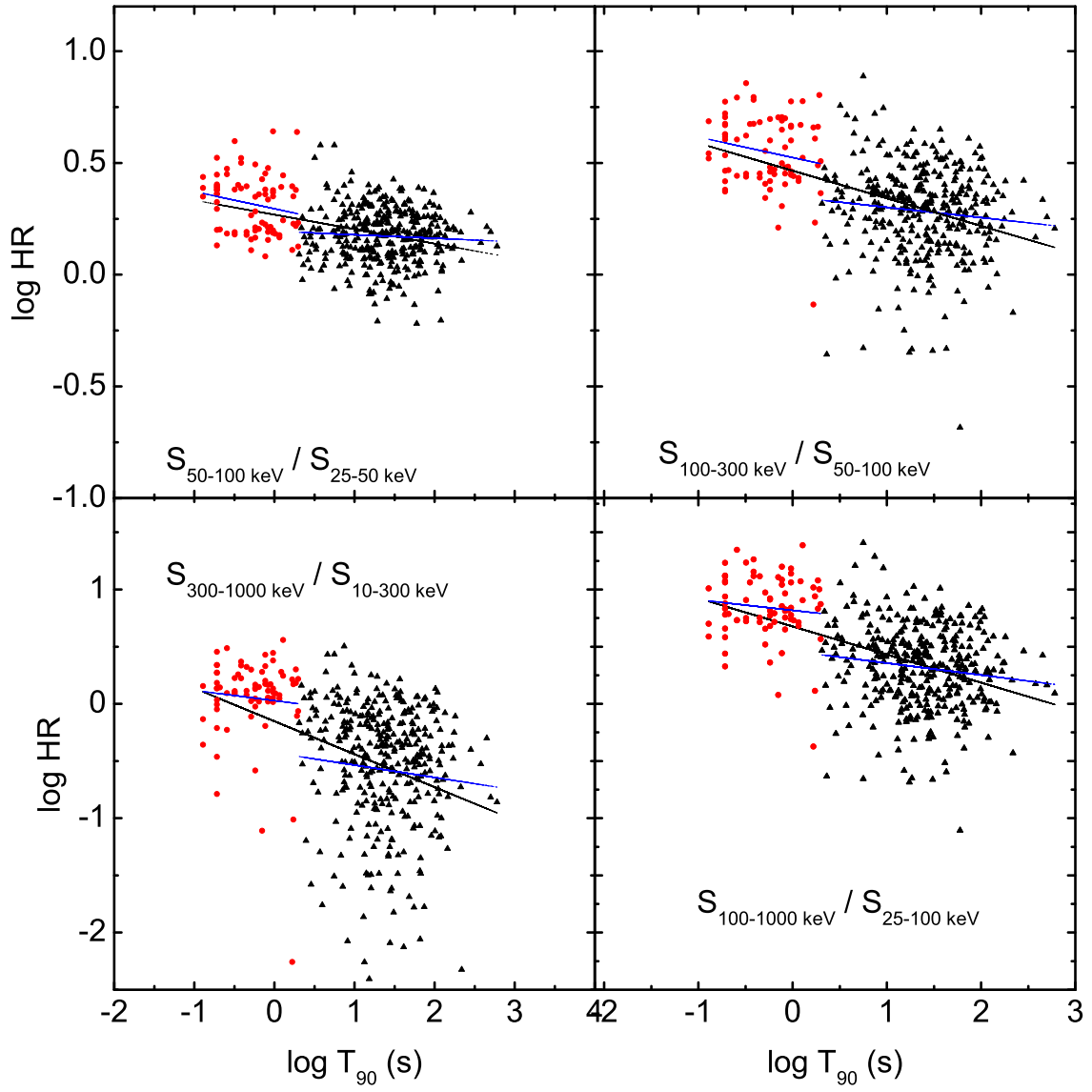


FIG. 2.— Hardness ratio *versus* duration for 425 Fermi GRBs. The filled circles represent the short GRBs and the filled triangles represent the long ones. The solid lines are the best fits for all bursts, the dashed lines are the best fits to short or long events separately. For clarity, the estimated errors are not shown.

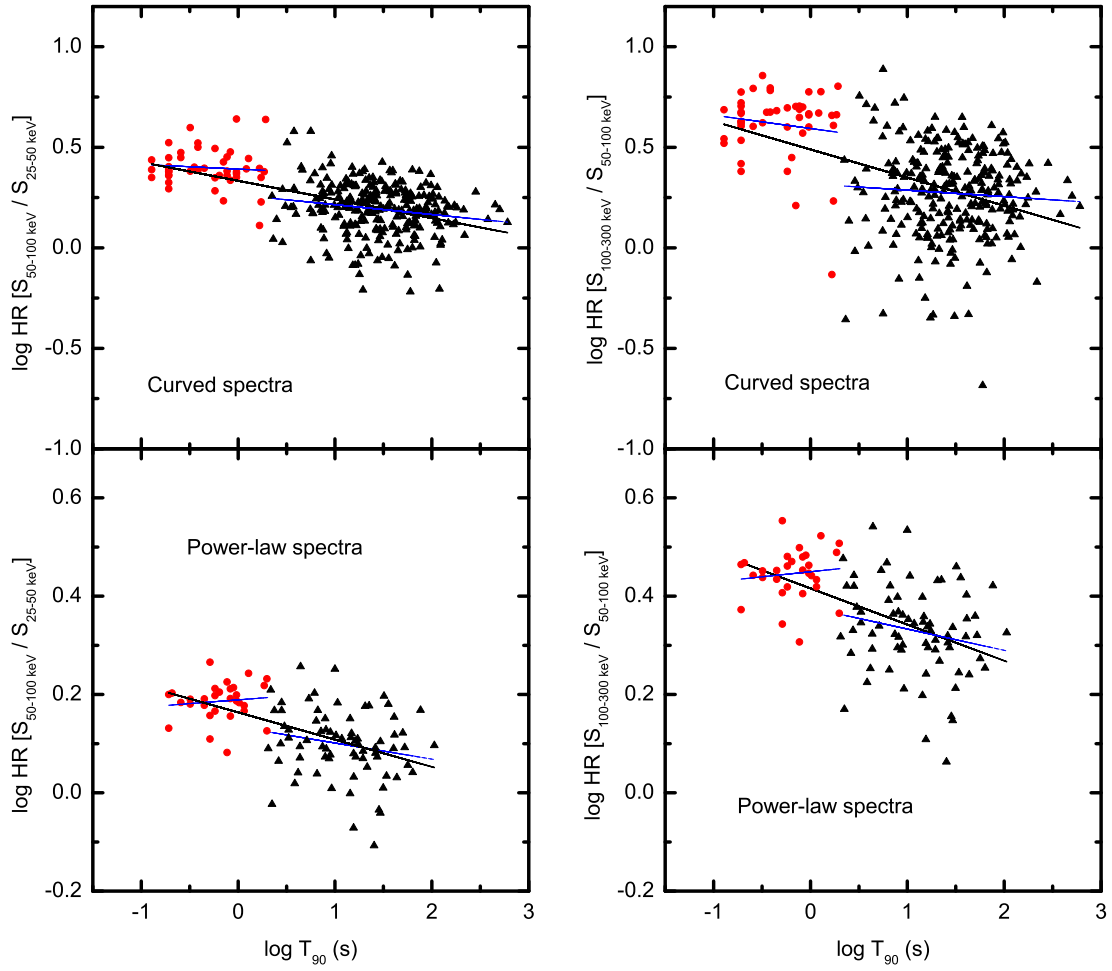


FIG. 3.— The correlation between hardness ratio and duration for GRBs with the different spectral shape. The other symbols are the same as Figure 2.



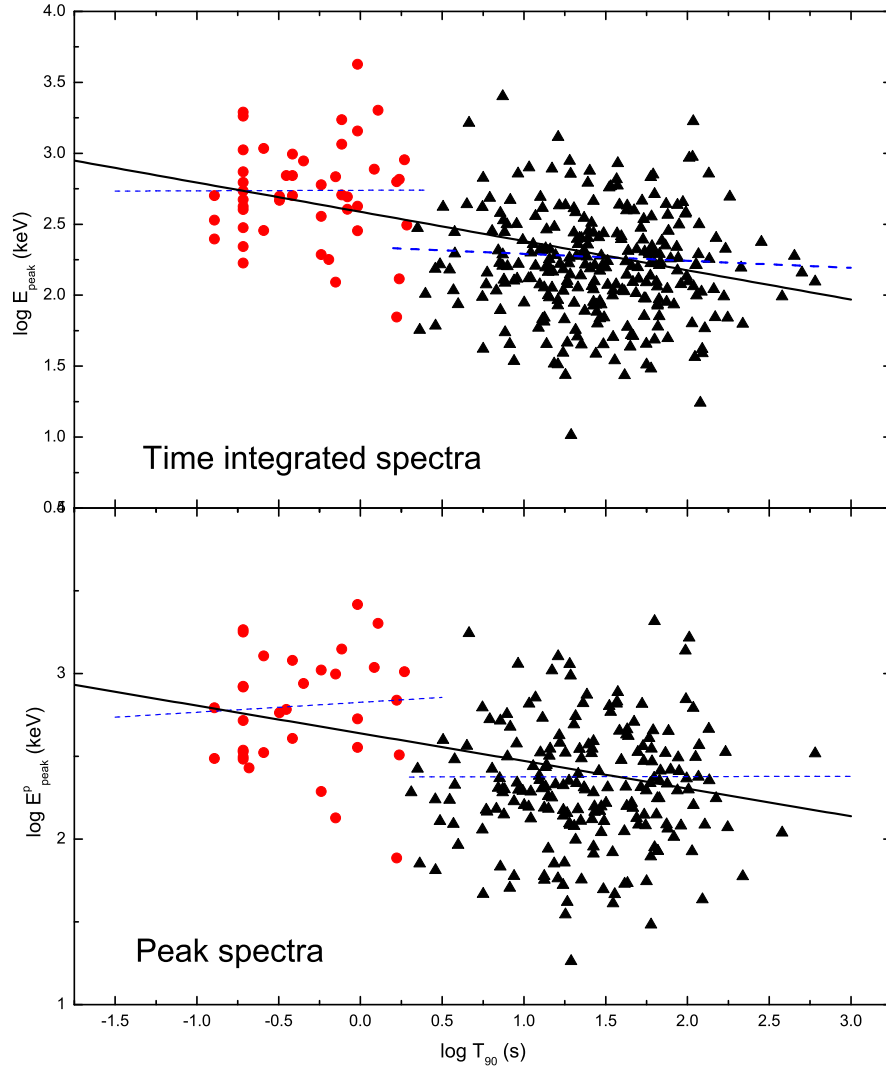


FIG. 4.— *Top*: The correlation between the observed peak energies in the time integrated spectra ( $E_{\text{peak}}$ ) and durations for 322 Fermi GRBs with the curved spectra. *Bottom*: The correlation between the peak energies in the peak flux spectra ( $E_{\text{peak}}^p$ ) and durations for 234 GRBs with the curved peak flux spectra. The other symbols are the same as Figure 2.

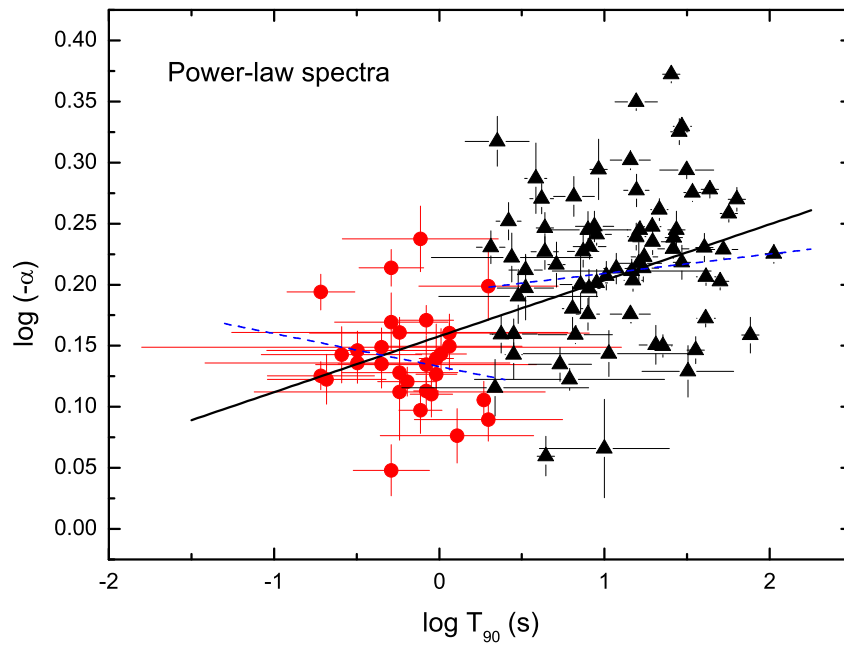


FIG. 5.— Distribution of the spectral indices ( $\alpha$ ) versus durations for 103 GRBs with the power-law spectra. The other symbols are the same as Figure 2.

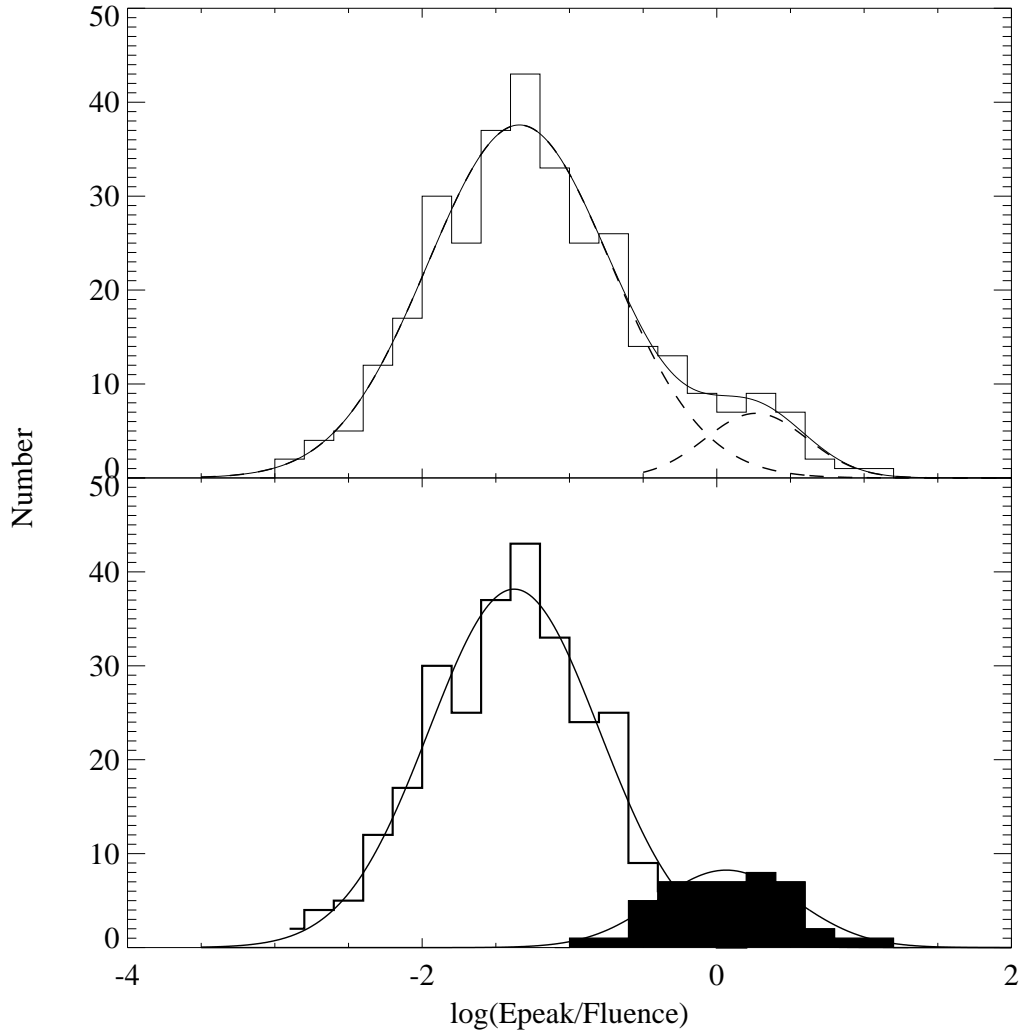


FIG. 6.— Distribution of the energy ratio ( $E_{\text{peak}}/\text{Fluence}$ ), where the fluence is measured in the 10–1000 keV energy range. Top panel shows the distribution for all 322 GRBs with the curved spectra. The dashed lines are the best fits with two log-normal functions separately and the solid line represent the superpositions of two log-normal fitting. Bottom panel shows the distribution for 275 long GRBs (unfilled histogram) and 47 short GRBs (filled histogram), where the solid curves are the best-fit log-normal functions. There are clearly two distinct distributions.

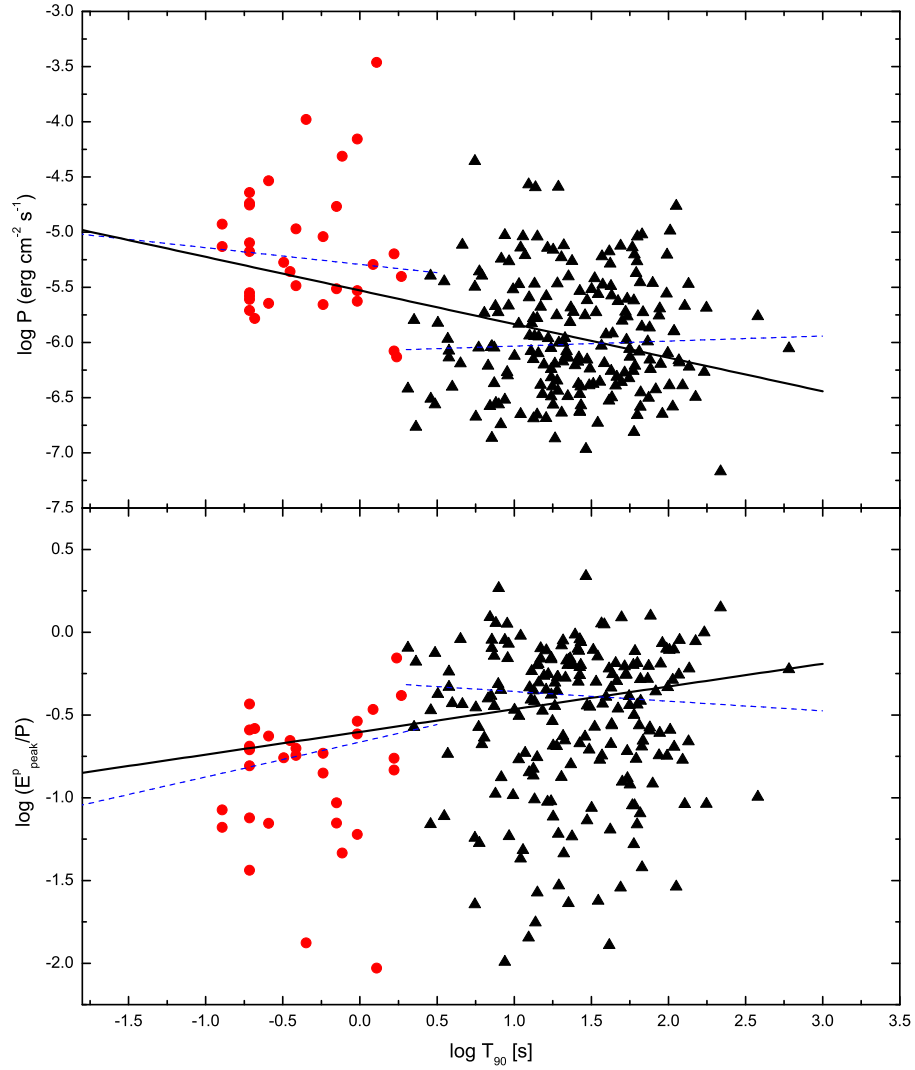


FIG. 7.— The correlations between the peak flux ( $P$ ) and the duration ( $T_{90}$ ), and between the  $E_{\text{peak}}^p/P$  ratio and  $T_{90}$  for 234 GRBs with the curved peak flux spectra, where  $E_{\text{peak}}^p$  is the peak energy in the peak flux spectra of a GRB. The other symbols are the same as Figure 2.

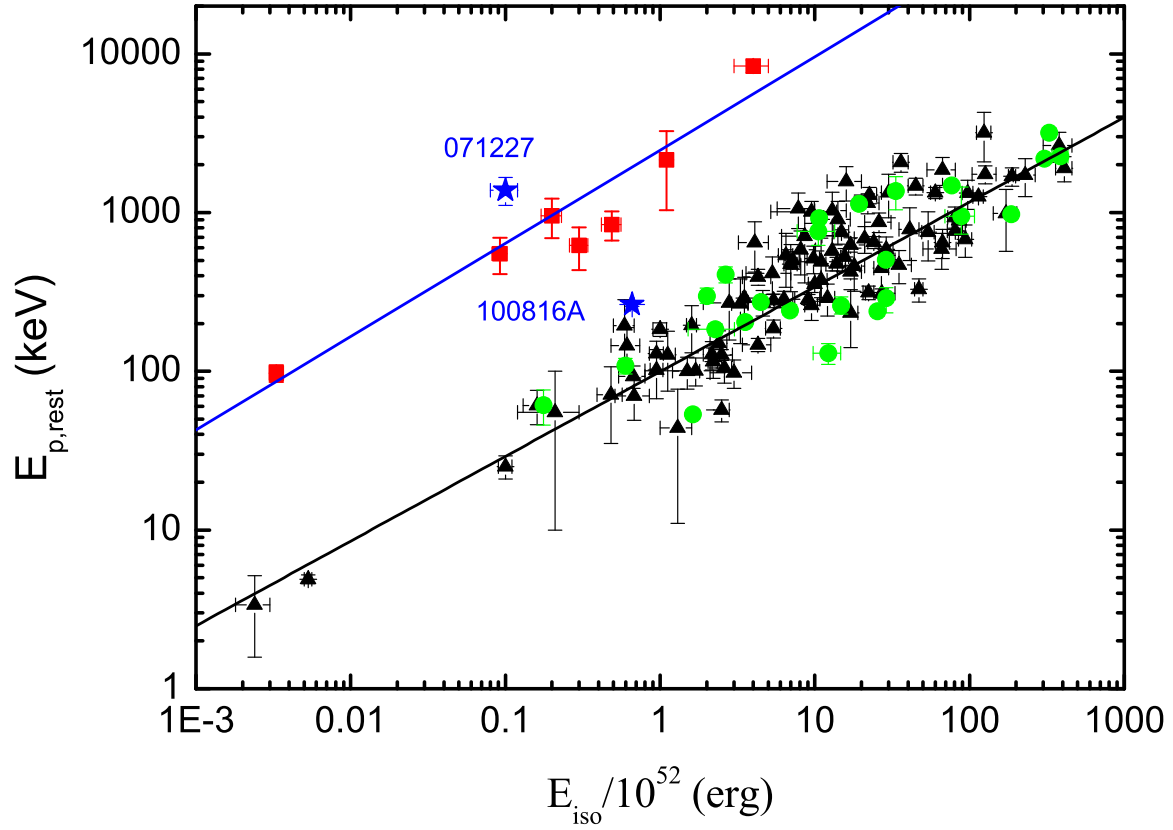


FIG. 8.— The correlations between the rest frame peak energy ( $E_{p,\text{rest}}$ ) and the isotropic total energy ( $E_{\text{iso}}$ ). The squares represent the short GRBs, the triangles represent Pre-Fermi long GRBs taken from Amati et al. (2010) and the references therein, and the circles represent Fermi long GRBs listed in Table 3. The stars are the two controversial GRBs, GRB 071227 and GRB 100816A. The solid lines are the best fit correlations:  $E_{p,\text{rest}} = 2455 \times \left(\frac{E_{\text{iso}}}{10^{52}}\right)^{0.59}$  for short GRBs and  $E_{p,\text{rest}} = 100 \times \left(\frac{E_{\text{iso}}}{10^{52}}\right)^{0.51}$  for long GRBs.

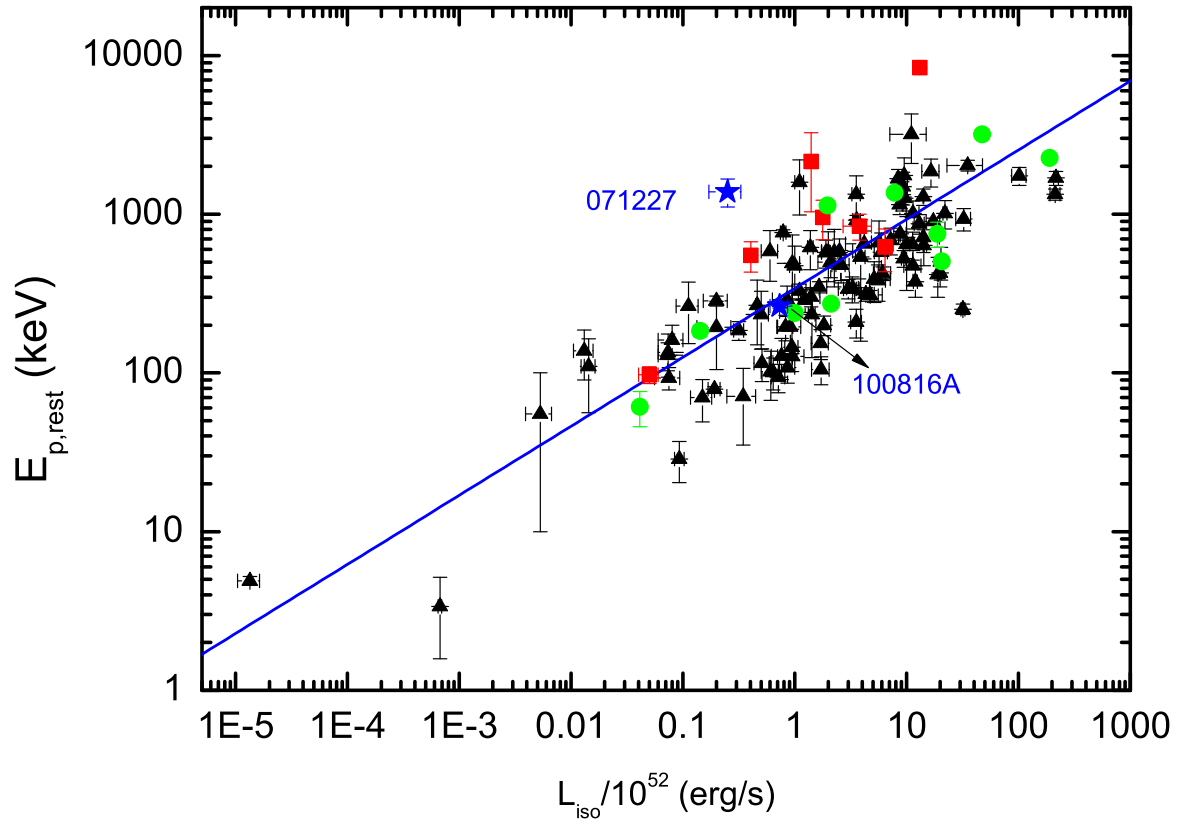


FIG. 9.— The correlation between the rest frame peak energy ( $E_{p,\text{rest}}$ ) and the isotropic peak luminosity ( $L_{\text{iso}}$ ), where the 105 long GRB data are taken from Ghirlanda et al. 2010 and the references therein. The other symbols are the same as Figure 8. Combined short and long GRBs, the best fit to the  $E_{p,\text{rest}} - L_{\text{iso}}$  correlation yield  $E_{p,\text{rest}} = 302 \times \left(\frac{L_{\text{iso}}}{10^{52}}\right)^{0.40 \pm 0.03}$ .

TABLE 1  
CORRELATION ANALYSIS RESULTS.

Data*	Number	HR*	$a$	$b$	$r$	Probability
$\log(HR) = a + b \log(T_{90})$						
All	425	HR1	0.27±0.01	-0.06±0.01	-0.28	$5.2 \times 10^{-9}$
All	425	HR2	0.47±0.02	-0.12±0.01	-0.41	$2.8 \times 10^{-18}$
All	425	HR3	-0.15±0.05	-0.29±0.04	-0.42	$6.2 \times 10^{-20}$
All	425	HR4	0.68±0.03	-0.25±0.02	-0.44	$3.0 \times 10^{-21}$
Short	77	HR1	0.30±0.02	-0.08±0.04	-0.22	0.06
Short	77	HR2	0.52±0.02	-0.09±0.05	-0.13	0.25
Short	77	HR3	0.03±0.06	-0.09±0.13	0.04	0.74
Short	77	HR4	0.82±0.04	-0.09±0.10	-0.03	0.81
Long	348	HR1	0.19±0.02	-0.02±0.01	-0.03	0.56
Long	348	HR2	0.35±0.03	-0.05±0.02	-0.11	0.03
Long	348	HR3	-0.43±0.11	-0.11±0.07	-0.14	0.009
Long	348	HR4	0.46±0.06	-0.10±0.04	-0.15	0.007
S1 All	322	HR1	0.33±0.01	-0.09±0.01	-0.44	$8.4 \times 10^{-17}$
S2 All	103	HR1	0.16±0.01	-0.05±0.01	-0.55	$1.5 \times 10^{-9}$
S1 All	322	HR2	0.49±0.02	-0.14±0.02	-0.36	$2.2 \times 10^{-11}$
S2 All	103	HR2	0.42±0.01	-0.07±0.01	-0.55	$1.5 \times 10^{-9}$
S1 Short	47	HR1	0.39±0.02	-0.02±0.04	-0.09	0.56
S2 Short	30	HR1	0.19±0.01	0.02±0.03	0.16	0.40
S1 Short	47	HR2	0.59±0.04	-0.07±0.07	0.05	0.72
S2 Short	30	HR2	0.45±0.01	0.02±0.03	0.16	0.40
S1 Long	275	HR1	0.26±0.03	-0.05±0.02	-0.18	0.003
S2 Long	73	HR1	0.13±0.02	-0.03±0.02	-0.20	0.09
S1 Long	275	HR2	0.32±0.04	-0.03±0.03	-0.07	0.23
S2 Long	73	HR2	0.38±0.03	-0.04±0.02	-0.20	0.09

\* S1 represents *sample 1* (316 GRBs with the curved spectra) and S2 represents *sample 2* (108 GRBs with the power-law spectra).

\* The hardness ratios ( $HR$ ) are measured between two different energy bands, namely  $HR1$ , between the 50-100 keV and the 25-50 keV energy bands, i.e. the typical BAT energy bands;  $HR2$ , between the 100-300 keV and the 50-100 keV energy bands, i.e. the typical BATSE energy bands;  $HR3$ , between the 300-1000 keV and the 10-300 keV energy bands; and  $HR4$ , between the 100-1000 keV and the 25-100 keV energy bands.

TABLE 2  
CORRELATION ANALYSIS RESULTS.

Data*	Number	$a$	$b$	$r$	Probability
$\log(E_{\text{peak}}) = a + b \log(T_{90})$					
S1 All	322	2.59±0.03	-0.21±0.03	-0.30	6.6×10 <sup>-8</sup>
S1 Short	47	2.74±0.07	0.01±0.13	0.08	0.59
S1 Long	275	2.34±0.08	-0.05±0.05	-0.05	0.42
$\log(E_{\text{peak}}^{\text{p}}) = a + b \log(T_{90})$					
S3 All	234	2.64±0.04	-0.17±0.03	-0.22	7.0×10 <sup>-4</sup>
S3 Short	33	2.83±0.08	0.06±0.15	0.14	0.42
S3 Long	201	2.37±0.09	0.01±0.06	0.02	0.79
$\log(-\alpha) = a + b \log(T_{90})$					
S2 All	103	0.16±0.01	0.05±0.01	0.55	1.5×10 <sup>-9</sup>
S2 Short	30	0.13±0.01	-0.03±0.02	-0.16	0.40
S2 Long	73	0.19±0.02	0.02±0.02	0.20	0.09
$\log(P) = a + b \log(T_{90})$					
S3 All	234	-5.53±0.05	-0.30±0.04	-0.25	9.0×10 <sup>-5</sup>
S3 Short	33	-5.29±0.12	-0.15±0.23	-0.09	0.61
S3 Long	201	-6.08±0.11	0.05±0.07	0.003	0.97
$\log(E_{\text{peak}}^{\text{p}}/P) = a + b \log(T_{90})$					
S3 All	234	-0.60±0.04	0.14±0.03	0.18	0.006
S3 Short	33	-0.66±0.08	0.21±0.16	0.10	0.59
S3 Long	201	-0.30±0.09	-0.06±0.06	0.01	0.85
$\log(E_{\text{p,rest}}) = a + b \log(E_{\text{iso}}/10^{52})$					
Short	7	3.39±0.04	0.59±0.04	0.89	6.8×10 <sup>-3</sup>
Long	110	2.00±0.01	0.51±0.03	0.85	1.2×10 <sup>-31</sup>
$\log(E_{\text{p,rest}}) = a + b \log(L_{\text{iso}}/10^{52})$					
	112	2.48±0.03	0.40±0.03	0.76	2.3×10 <sup>-23</sup>

\* S1, S2 and S3 represent *sample 1* (322 GRBs with the curved spectra), *sample 2* (103 GRBs with the power-law spectra) and *sample 3* (234 GRBs with the curved peak flux spectra), respectively.

TABLE 3  
SHORT GRBs WITH MEASURED REDSHIFTS AND SPECTRAL PARAMETERS.

GRB	$z^*$	$\alpha$	Peak flux	Range (keV)	$L_{\text{iso}}$ 10 <sup>52</sup> erg/s	$E_{\text{p,rest}}$ (keV)	Fluence (10 <sup>-6</sup> )	range (keV)	$E_{\text{iso}}$ 10 <sup>52</sup> erg	Ref.
050709	0.16	-0.53±0.12	5.1±0.5E-6	2-400	0.05±0.01	97.4±11.6	0.4±0.04	2-400	0.0033±0.0001	1
051221	0.5465	-1.08±0.13	4.6±1.3E-5	20-2000	6.42±0.56	620±186	3.2±0.9	20-2000	0.3±0.04	1
061006	0.4377	-0.62±0.2	2.1e-5	20-2000	1.78±0.23	955±267	3.57	20-2000	0.2±0.03	1
070714	0.92	-0.86±0.1	2.8±0.3	100-1000	1.4±0.1	2150±1113	3.7	15-2000	1.1±0.1	1
090510	0.903	-0.80±0.03	80	8-40000	13.1±0.87	8370±760	30±2	8-40000	3.75±0.25	2
100117A	0.92	-0.14 <sup>+0.33</sup> <sub>-0.27</sub>	6.1±0.4	8-1000	0.41±0.05	551 <sup>+142</sup> <sub>-96</sub>	0.41±0.05	8-1000	0.09±0.01	3
101219A	0.718	-0.22 <sup>+0.30</sup> <sub>-0.25</sub>	2.8±0.8E-6	20-10000	3.78±1.08	842 <sup>+177</sup> <sub>-136</sub>	3.6±0.5	20-10000	0.49±0.07	4
071227*	0.383	-0.7	3.5±1.1E-6	20-1300	0.25±0.08	1384±277	1.6±0.2	20-1300	0.1±0.02	5

References: (1) Ghirlanda et al. (2008); (2) Guiriec et al. 2009 ; (3) Paciesas et al. 2010; (4) Golenetskii et al. 2010; (5) Golenetskii et al. 2007.

Notes. \* Some authors suggested that this GRB is a disguised short one as GRB 060614 (e.g., Caito et al. 2010).

\* The redshift are taken from the Greiner's webpage (<http://www.mpe.mpg.de/~jcg/grbgen.html>).



TABLE 4

THE SPECTRAL PARAMETERS OF 27 FERMI-GBM GRBS WITH KNOWN REDSHIFTS AND WELL MEASURED PEAK ENERGIES. THE REDSHIFT ARE TAKEN FROM THE GREINER'S WEBPAGE.

GRB	$z$	$\alpha$	$\beta$	$E_{\text{peak}}$ (keV)	Fluence ( $10^{-6}$ erg/cm $^2$ )	range (keV)	$E_{\text{iso}}$ ( $10^{52}$ erg)	GCN number
080810	3.35	-0.91±0.12	...	313.5±73.6	6.9±0.5	50-300	33.3±2.4	8100
080916A	0.689	-0.9±0.1	...	109±9	15±5	25-1000	2.27±0.76	8263
080916C	4.35	-0.91±0.02	-2.08±0.06	424±24	190	8-30000	387±46	8278
081007	0.5295	-1.4±0.4	...	40±10	1.2±0.1	25-900	0.18±0.02	8369
081222	2.77	-0.55±0.07	-2.1±0.06	134±9	13.5±0.8	8-1000	28.8±1.7	8715
090323	3.57	-0.89±0.03	...	697±51	100±1	8-1000	327±3	9035
090328	0.736	-0.93±0.02	-2.2±0.1	653±45	80.9±1	8-1000	19.3±0.2	9057
090423	8.26	-0.77±0.35	...	82±15	1.1±0.3	8-1000	10.6±2.9	9229
090424	0.544	-0.9±0.02	-2.9±0.1	177±3	52±1	8-1000	4.47±0.09	9230
090510 <sup>a</sup>	0.903	-0.8±0.03	-2.6±0.3	4400±400	30±2	8-40000	3.75±0.25	9336
090516	4.109	-1.51±0.11	...	185.6 <sup>+98.4</sup> <sub>-42.5</sub>	23±5	8-1000	88.5±19.2	9415
090618	0.54	-1.26 <sup>+0.06</sup> <sub>-0.02</sub>	-2.5 <sup>+0.15</sup> <sub>-0.33</sub>	155.5 <sup>+11.1</sup> <sub>-10.5</sub>	270±6	8-1000	25.4±0.6	9535
090902B	1.822	-0.70±0.01	-3.85 <sup>+0.21</sup> <sub>-0.31</sub>	775±11	374±3	50-10000	305±2	9866
090926A	2.1062	-0.75±0.01	-2.59 <sup>+0.04</sup> <sub>-0.05</sub>	314±4	145±4	8-1000	186±5	9933
090926B	1.24	-0.13±0.06	...	91±2	8.7±0.3	10-1000	3.55±0.12	9957
091003A	0.8969	-1.13±0.01	-2.64±0.24	486.2±23.6	37.6±0.4	8-1000	10.6±0.1	9983
091020	1.71	-0.2±0.4	-1.7±0.02	47.9±7.1	10±2	8-1000	12.2±2.4	10095
091127	0.49	-1.27±0.06	-2.2±0.02	36±2	18.7±0.2	8-1000	1.63±0.02	10204
091208B	1.063	-1.48 <sup>+0.05</sup> <sub>-0.05</sub>	...	144.2 <sup>+18</sup> <sub>-13.9</sub>	5.8±0.2	8-1000	2.01±0.07	10266
100117A <sup>a</sup>	0.92	-0.14 <sup>+0.33</sup> <sub>-0.27</sub>	...	287 <sup>+74</sup> <sub>-50</sub>	0.41±0.05	8-1000	0.09±0.01	10345
100414A	1.368	-0.58±0.01	...	627.6 <sup>+12.5</sup> <sub>-12.1</sub>	129±2	8-1000	76.6±1.2	10595
100728B	2.106	-0.9±0.1	...	131±15	2.4±0.1	8-1000	2.66±0.11	11015
100814A	1.44	-0.64 <sup>+0.14</sup> <sub>-0.12</sub>	-2.02 <sup>+0.09</sup> <sub>-0.12</sub>	106.4 <sup>+13.9</sup> <sub>-12.6</sub>	19.8±0.6	10-1000	14.8±0.5	11099
100816A <sup>b</sup>	0.8049	-0.31±0.05	-2.77±0.17	136.7±4.7	3.84±0.13	10-1000	0.73±0.02	11124
100906A	1.727	-1.34 <sup>+0.08</sup> <sub>-0.06</sub>	-1.98 <sup>+0.06</sup> <sub>-0.07</sub>	106 <sup>+17.5</sup> <sub>-20.2</sub>	26.4±0.3	10-1000	28.9±0.3	11248
101219B	0.55	0.33±0.36	-2.12±0.12	70±8	5.5±0.4	10-1000	0.59±0.04	11477
110213A	1.46	-1.44±0.05	...	98.4 <sup>+8.5</sup> <sub>-6.9</sub>	10.3±0.3	10-1000	6.9±0.2	11727

Notes. <sup>a</sup> Two short GRBs.

<sup>b</sup> This GRB was classified as a short one by the previous study (e.g., Gruber et al. 2011), we find it should belong to the long class.